Studies of the adsorption parameters of Gentian Violet onto Mango (Mangifera indica Lam) Shell Activated Carbons

I. A. Gouré bi, B.G.H. Briton, Y. Soro*, B.K. Yao

Laboratoire des Procédés Industriels de Synthèse, de l'Environnement et des Energies Nouvelles (LAPISEN), Institut National Polytechnique Félix HOUPHOUËT-BOIGNY de Yamoussoukro, BP 1093 Yamoussoukro, Côte d'Ivoire

Corresponding author: E-mail : yaya.soro@inphb.ci

Abstract

Two activated carbons (ACs) were prepared by chemical activation of mango shells with phosphoric acid (AC-A) or sodium hydroxide (AC-BN) at 600 °C for 2 hours. Specific surface area, surface functions, zero charge point of pH (pHzpc) and morphology of the adsorbents were also determined. With specific surfaces of 270 m2 g-1 for AC-A and 421 m2 g-1 for AC-BN, these adsorbents were used for removing Gentian violet in aqueous solution in a batch reactor stirred magnetically at a speed of 150 rpm. Thus, the contact time, the hydrogen potential of the solution, the temperature of the reaction medium and dose of the adsorbent were analyzed. The elimination of Gentian violet on both ACs was well described by a pseudo-second order kinetics with a regression coefficient close to 1 (R2 > 0.999). The Gentian violet adsorption was perfectly described by Freundlich isotherm with higher determination coefficients for AC-A (R2 > 0.99) and AC-BN (R2 > 0.98) and by pseudo-second order kinetics. The Gentian violet adsorption was characterized by a multilayer on the activated carbon surface. AC-A and AC-BN were effective in removing the Gentian violet respectively with maximum adsorption capacities of 128.04 mg g-1 and 140.65 mg g-1.

1. Introduction

Industrialization which is supposed to solve unemployment problem due to high population growth in developing countries, is generally not accompanied by an environmental policy to such an extent that some industries discharge their wastewater directly into the surface water [1]. This wastewater, loaded with non-biodegradable organic compounds such as textile dyes, considerably deteriorates the physicochemical quality of the receiving environments [2]. This wastewater is also responsible for the disruption of photosynthesis of algae or the contamination of aquatic species leading to the death of these ones due to chronic or acute toxicity [3,4]. For example, the Gentian Violet (GV) that is used in the textile industry because of its high solubility in water [5], is toxic, carcinogenic and can lead to kidney failure [6].

Thus, several water treatments processes such as membrane filtration [4], advanced oxidation processes [7], electrocoagulation [8], and adsorption on porous materials [9] have been implemented to remove recalcitrant pollutants. Adsorption on porous materials and particularly on activated carbons from lignocellulosic biomass remains today the least expensive treatment process in its design and implementation [10]. Thus, activated carbon from palm fibers [11], coconut shells [12], peanut shells

[13], sawdust [14], date stones [15], stem from the banana bunch [1] have been used in the removal of dyes from industrial wastewater.

Mango shells are available and abundant agricultural by-products in Côte d'Ivoire, the leading African producer of mangoes and the world's third largest exporter after Peru and Brazil, with an estimated mango production of 155,000 tons/year [16]. Despite some studies of oil production and biomolecules isolation from kernel seed cake of the mango [17-19] or corn substitution trials in poultry and ruminant feed [20], these mango shells are poorly valued. Recently, they have been used to produce modified or unmodified activated carbon to remove acetone vapor [21], phenol from wastewater [22], methylene blue in aqueous solution [23], and to adsorb crude oil [24].

The present work aims to prepare activated carbons from the shells of mango kernels of the Adams variety by acid or basic activation in order to remove the Gentian Violet dye in aqueous solution.

2. Materials and Methods

2.1 Vegetal material

Mango fruits were collected in April 2017 at the end of dry season in Yamoussoukro (6047'18.762" N and 5015'25.9992" W) in the center of Côte d'Ivoire. Mango kernels (**Figure 1a**) were isolated from the fruits and dried in the sun for two weeks and then the seed were separated from the shells. The resulting mango shells (**Figure 1b**) were stored in the laboratory until used to prepare activated carbons (ACs).

Figure 1. Mango kernel **(a)**, Mango shells **(b)**

2.2 Preparation of activated carbons

Dry mango shells were crushed into small particles in a grinder and then impregnated in aqueous solutions of phosphoric acid (85% purity; Aldrich) or sodium hydroxide (Aldrich) at 1/3 ratios (g mango shells/g H_3PO_4 or NaOH) for 24 hours. Each impregnated solid residue was drained and then oven dried overnight in a desiccator at 80 °C. The carbonization of the impregnated solid residue contained in a well-closed stainless-steel crucible had been carried out at 600 °C without air renewal in a muffle furnace set at 10 °C/min for two hours. The resulting carbonized residue was washed several times in distilled water to remove the excess phosphoric acid or sodium hydroxide before being oven dried at 105 °C for 24 hours. Charcoals activated with phosphoric acid and sodium hydroxide were respectively designated AC-A and AC-BN.

2.3 Adsorbent analysis methods

The specific surface area, pore volume and pore size distribution of the activated carbons were determined according to the N$_2$ adsorption-desorption isotherm at 77 K using the Micromeritics ASAP 2020 type sorptometer. The specific surface area was determined according to the Brunauer, Emmett and Teller (BET) method. The pore size distribution was determined by the Barett-Joyner-Halenda method [25]. The total pore volume (V$_{tot}$) was determined by considering the quantity of N$_2$ adsorbed at the relative pressure (P/P°) around 0.99. Mesoporous volume was the difference between total volume and microporous volume. The average pore diameter (d$_p$) was obtained according to **Eqn. 1** [26].

$$d_p = \frac{4V_{tot}}{S_{BET}} \qquad\qquad \textbf{Eqn. 1}$$

The surface morphology of the adsorbents was analysed by a 40 VP Zeiss Supra type scanning electron microscope (SEM). The functional groups were identified using a Fourier Transform Infrared (FTIR) spectrometer (Nicolet iS10 brand). Germanium crystal was used as a sample support using the Attenuated Total Reflectance (ATR) method. The absorbance intensities were recorded at wavelengths between 400 and 4000 cm^{-1}.

The zero charge point of pH (pHzpc) of ACs was determined by placing seven (7) Erlenmeyer flasks each containing 50 mL of 0.1 M NaCl. After adjusting the pH from 2 to 12 with HCl (0.1 M) and NaOH (0.1 M) solutions, 0.05 g of AC-A or AC-BN was added. A stirring at 60 rpm had been carried out in a water bath for 24 hours to maintain the ACs particles dispersion in the solution. Then the final pH values recorded were plotted according to the initial pH values. The pHzpc is the intersection point of the resulting curve with the first bisector [27].

2.4 Adsorption studies

The contact time was carried out in batch mode on 100 mL of an aqueous solution of GV at 50 mg L^{-1} in the presence of 0.1 g of AC-A or AC-BN in an Erlenmeyer flask at pH 7.2. The reaction mixtures put in a water bath were stirred at 150 rpm at room temperature (28 ± 2 °C). Every 10 minutes, 1 mL of the reaction mixture was removed, then diluted and centrifuged at 3500 rpm. The supernatant was then analysed with a UV visible spectrophotometer at 592 nm in order to determine the residual concentration. After determining the equilibrium time from the previous experiments, the adsorption isotherms were carried out in the presence of 0.1 g of the activated carbon for 150 min at different initial concentrations of GV (50 - 500 mg L^{-1}).

Effect of the initial pH (2 - 10) was studied at room temperature on 100 mL of GV at 50 mg L^{-1} in the presence of 0.1 g of adsorbent for 150 min. These pHs were adjusted with aqueous solutions of HCl (0.1M) or NaOH (0.1M) and then measured using a pH meter (HANNA HI 8424). The effect of adsorbent dose (0.05 - 0.4 g) was also studied at room temperature (28 ± 2 °C) on 100 mL of GV (50 mg L^{-1}) at 150 rpm for 150 min. Finally, in this same thermostatically controlled bath, a temperature variation (25 - 55 °C) made it possible to study the effect of this parameter on the GV adsorption capacity by these two activated carbons. In fact, these experiments were carried out in the presence of 0.1 g of each adsorbent in 100 mL of GV (50 mg L^{-1}) at 150 rpm for 150 min. The adsorption percentage (Γ in %) and the equilibrium adsorption capacity (q$_e$ in mg g^{-1}) of GV by the ACs were determined from the **Eqn. 2** and **3**.

$$\Gamma(\%) = \left(1 - \frac{C_e}{C_0}\right) * 100 \qquad\qquad \textbf{Eqn. 2}$$

$$q_e = \frac{(C_0 - C_e)V}{m} \qquad \qquad \textbf{Eqn. 3}$$

Where C_0 (mg L^{-1}) and C_e (mg L^{-1}) are respectively the initial concentration and that of the adsorbate at time t ; V (L) is the volume of the solution and m (g) is the mass of the adsorbent.

The GV adsorption on ACs was modeled by pseudo-first order (**Eqn. 4**) and pseudo-second order (**Eqn. 5**) kinetics, then by intraparticle diffusion (**Eqn. 6**) [2].

$$q_t = q_e\left(1 - e^{-k_1 t}\right) \qquad \qquad \textbf{Eqn. 4}$$

$$q_t = \frac{k_2 q_e^2 t}{1 + k_2 q_e t} \qquad \qquad \textbf{Eqn. 5}$$

$$q_t = k_i t^{1/2} + C \qquad \qquad \textbf{Eqn. 6}$$

Where q_t (mg g^{-1}) and q_e (mg g^{-1}) are respectively the adsorbed quantities at a given time t and at equilibrium, k_1 (min^{-1}) and k_2 (g mg^{-1} min^{-1}) are the respective pseudo-first order and pseudo-second order rate constants. k_i (mg g^{-1} min$^{-1/2}$) is the intraparticle diffusion rate constant and C (mg g^{-1}) is a constant that provides information on the thickness of the boundary layer. The graphical representations of ln(q_e - q_t) and t/q_t as a function of t is used in order to determine k_1, k_2 and q_e. Finally, k_i and C are determined by plotting q_t as a function of $t^{1/2}$.

Adsorption isotherms are essential for understanding the GV adsorption mechanism by ACs. In this study, Langmuir (**Eqn. 7**) and Freundlich (**Eqn. 8**) models were used to exploit the GV initial concentration data variation [28]. Indeed, Langmuir's model assumes monolayer adsorption at the adsorbent surface whereas Freundlich's model describes heterogeneous surfaces with different energy sites [29].

$$\frac{C_e}{q_e} = \frac{1}{q_m K_L} + \frac{C_e}{q_m} \qquad \qquad \textbf{Eqn. 7}$$

$$\ln q_e = \ln K_F + \frac{1}{n}\ln C_e \qquad \qquad \textbf{Eqn. 8}$$

Where q_m (mg g^{-1}) expresses the maximum adsorption capacity, K_L (L mg^{-1}) is Langmuir's constant, K_F (mg g^{-1}(L mg^{-1})$^{1/n}$) and 1/n are Freundlich constants linked respectively to adsorption capacity and adsorption intensity.

For Langmuir isotherm, the separation factor (R_L) is used to appreciate the adsorption process. This process may be irreversible (R_L tends towards 0), favourable (0 <R_L <1), linear (R_L = 1) or unfavourable (R_L> 1) [28]. R_L is defined by the expression of **Eqn. 9**.

$$R_L = \frac{1}{1 + K_L C_o} \qquad \qquad \textbf{Eqn. 9}$$

Where C_0 (mg L^{-1}) is the GV initial concentration and K_L is Langmuir's constant (L mg^{-1}).

The Chi-squared test (χ^2) was used to study the best fit of the adsorption isotherms. Indeed, χ^2 describes the variation between the calculated ($q_{e.cal}$) and experimental ($q_{e.exp}$) data as shown by the **Eqn. 10**:

$$\chi^2 = \sum \frac{(q_{e,exp} - q_{e,cal})^2}{q_{e,cal}} \qquad \qquad \textbf{Eqn. 10}$$

where $q_{e,cal}$ (mg g^{-1}) and $q_{e,exp}$ (mg g^{-1}) are respectively the calculated equilibrium adsorption capacity and that obtained experimentally from the model. If the model data are well adjusted to the experimental, χ^2 is small; otherwise, it is larger [30].

2-5 Thermodynamics of adsorption reaction

Thermodynamic parameters, such as standard free enthalpy (ΔG^0), enthalpy (ΔH^0) and entropy (ΔS^0) variations, were evaluated by considering temperature effect (T) (25; 35; 45 and 55 °C) on GV adsorption by ACs. Thus, the values of ΔG^0 can be calculated according to the **Eqn. 11** where K_c is the absorption equilibrium constant (**Eqn. 12**) [31]:

$$\Delta G^o = -RTlnK_c \qquad\qquad \textbf{Eqn. 11}$$

$$K_C = \frac{C_0 - C_e}{C_e} \qquad\qquad \textbf{Eqn. 12}$$

(C_0 - C_e) and C_e are the equilibrium adsorption concentrations of GV on the adsorbent surface and in aqueous solution, respectively.

ΔH^0 and ΔS^0 were respectively determined from the slope and the interception of the line lnK_c as a function of $1/T$ (**Eqn. 13**):

$$lnK_C = \frac{\Delta S^o}{R} - \frac{\Delta H^o}{RT} \qquad\qquad \textbf{Eqn. 13}$$

Where R is the ideal gas constant (8.314 J mol^{-1} K^{-1})

3. Results and discussion

3.1 Textural properties of activated carbons

Figure 2, relating to the adsorption-desorption of N_2, shows that the obtained isotherms are of type IV according to the IUPAC classification, each with a type H_3 hysteresis loop. For AC-A, this hysteresis loop with a tray up to $P/P^0 \approx 1.0$ characterizes the simultaneous presence of micropores (pore diameter less than 2 nm) and mesopores (pore diameter between 2 and 50 nm) [32].
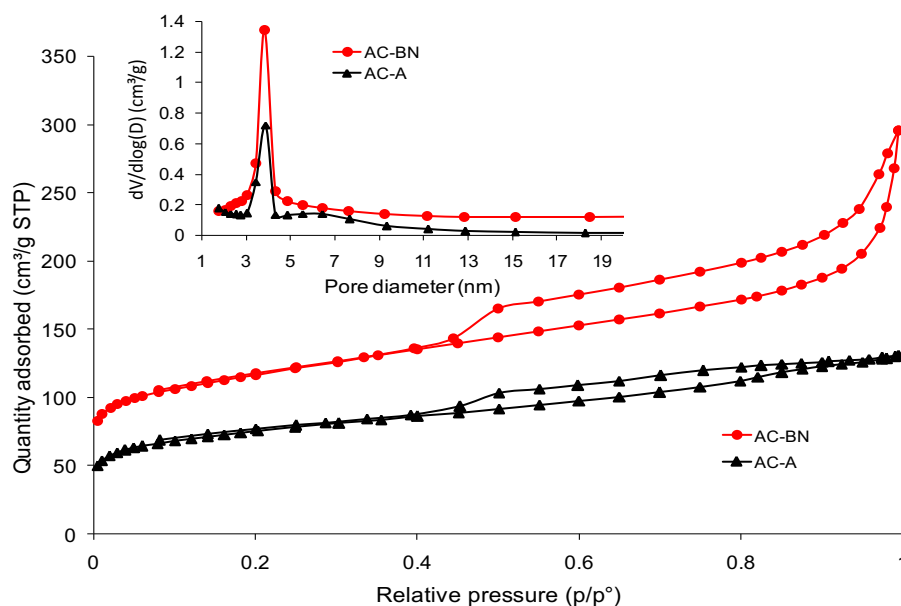

Figure 2. N$_2$ adsorption-desorption isotherms of the activated carbons (inserted graph: pore size distribution estimated from the BJH method).

Besides, for AC-BN, an increase in N_2 adsorption from P/P^0 greater than 0.8 is related to the existence of mesopores and macropores [32]. In addition, the pore size distributions (inserted graph in **Figure 2**) showed the presence of a maximum peak centered between 3 and 5 nm for each activated carbon. This reveals that the total volume of the pores is mainly represented by the mesopores as shown by the data in **Table 1**. Indeed, there are 30% of macropores and 64.75% of mesopores on the surface of AC-BN while that of AC-A is occupied by 87% of mesopores and about 10% of micropores. Thus, AC-BN is macro/mesoporous while AC-A is micro/mesoporous. Regarding adsorption efficiency, the prognosis could be in favour of AC-BN for its specific surface area of around 421 m^2 g^{-1} compared to 270 m^2 g^{-1} for AC-A.

Table 1. Textural properties of the activated carbons

| ACs	V_{micro} (cm^3/g)	V_{meso} (cm^3/g)	V_{macro} (cm^3/g)	V_t (cm^3/g)	S_{BET} (m^2/g)	$d_{average}$ (nm)	pHzpc
AC-A	0.015	0.135	0.005	0.155	270	2.29	2.3
AC-BN	0.019	0.248	0.116	0.383	421	3.63	6.6

3.2 Surface chemical properties

FTIR spectroscopy (**Figure 3**) was used to determine the surface functions of the various ACs. Analysis of functional groups on the surface of each activated carbon revealed the presence of absorption peaks. The broad band around 3054 cm^{-1} is characteristic of the O–H elongation vibration of phenolic groups and chemisorbed water. Peaks around 1617 cm^{-1} are typical of the C=C stretch vibration confirming the presence of aromatic rings in the structure of AC-A and AC-BN. The sharp band observed at 1288 cm^{-1} is attributed to the elongation vibration of the C–O bond. The bands at 1112 cm^{-1} (AC-A) and at 1013 cm^{-1} (AC-BN) are attributed to asymmetric elongation of C-O-C. The sharp band at 813 cm^{-1} (AC-A) corresponds to the out-of-plane deformation vibration of the C-H bonds of aromatic rings [1]. The spectra analysis in **Figure 3** shows that AC-A exhibits more absorption bands than AC-BN because of the impact of sodium hydroxide which has virtually destroyed some surface functions.
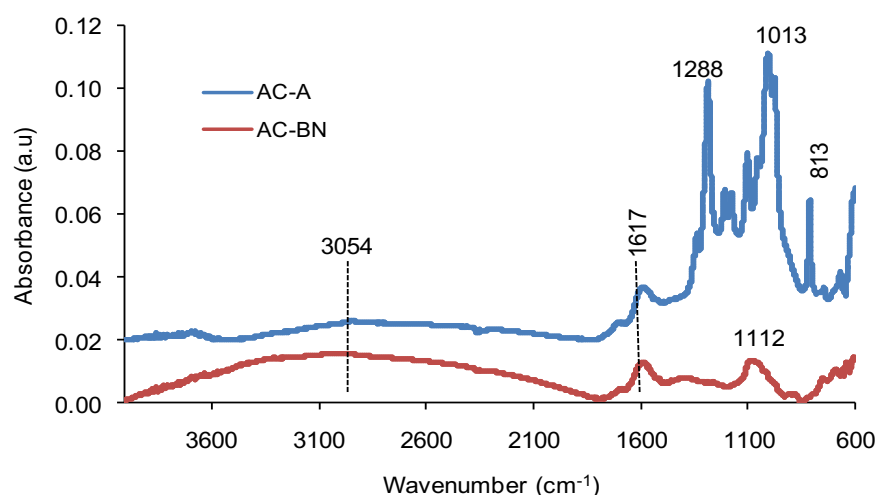
Figure 3. FTIR spectra of AC-A and AC-BN

3.3 Morphology of the two activated carbons

SEM images of AC-A and AC-BN at the 10 nm scale (**Figure 4**) were used to visualize the surface degradation on both sides because of the effect of activating agents. This resulted in a distribution of various irregular cavities [14] because the volatile organic substances were decomposed and evaporated during the carbonization process. The morphology of AC-BN shows the impact of sodium hydroxide that has virtually destroyed some surface functions. In addition, the fact of washing the two ACs several times with distilled water removed mineral impurities embedded in the porosity. The roughness of the surfaces of these activated carbons is also observed. This roughness has the advantage of promoting the retention of pollutants in aqueous solution.
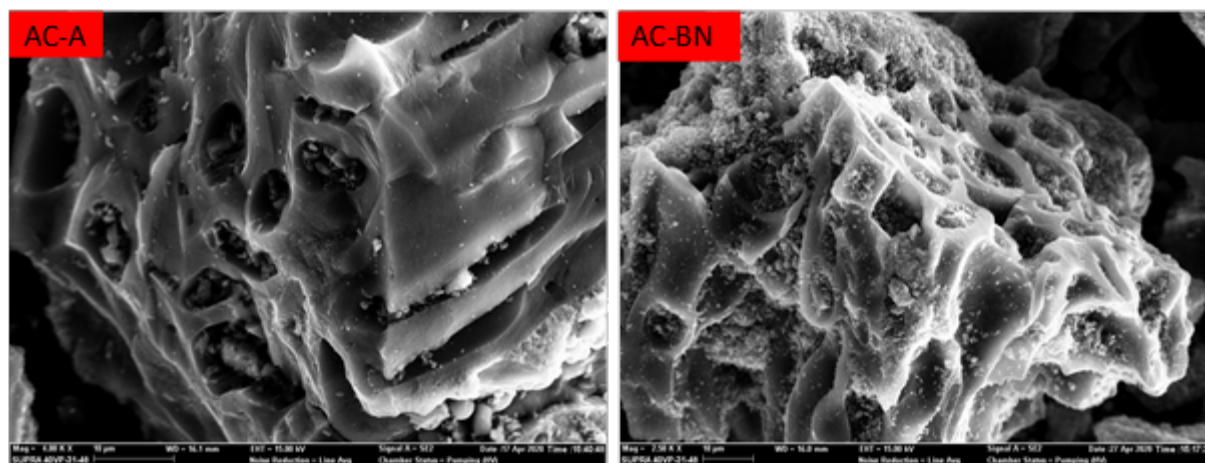

Figure 4. SEM images of AC-A (Mag = × 4,000 ; scale = 10 µm) and AC-BN (Mag = × 2,500 ; scale = 10 µm)

3-4 Effects of factors on dye adsorption

3-4-1 Effect of contact time

Figure 5 shows the effects of contact time on GV adsorption by ACs. Both curves show a rapid growth up to 30 minutes, what means the rapid elimination of GV on both ACs following progressive filling of the pores to reach saturation after 90 min for AC-A and 120 min for AC-BN. Indeed, at the beginning of the reaction, there are several available adsorption sites and which may be accessible to GV molecules [33]. The adsorption rates of around 90% for AC-A versus 62% for AC-BN show the effectiveness of AC-A compared to AC-BN. The best adsorption capacity of AC-A could be ascribed to the experimental conditions related to the initial pH (7.2). In further work, the adsorption equilibrium time was set at 150 min for the two ACs.
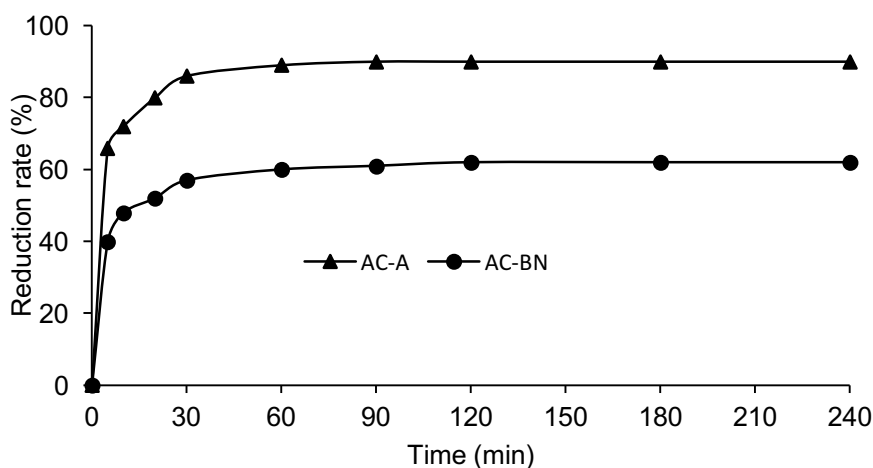
Figure 5. Effect of contact time on adsorption of GV by ACs (C_0 = 50 mg L^{-1} GV, m_{AC} = 0.1 g, pH = 7.2, T = 25 °C, V = 100 mL)

3-4-2 Effect of pH

Figure 6 shows the effect of pH on the GV reduction rate by ACs. According to this graph, GV reduction rate changes from 49% to 95.5% for AC-A (pHzpc = 2.3) when the pH of the reaction medium goes from 2 to 10 while for AC-BN (pHzpc = 6.6), the elimination peak is reached at pH = 6 with 91% efficiency before gradually decreasing to 38% for a pH = 10. The influence of the pH of the solution has been exploited to better understand the adsorption mechanism of this cationic dye. Indeed, both activated carbons having differently been activated with phosphoric acid and sodium hydroxide, the GV removal efficiency may be closely related to pHzpc because of electrostatic interactions. Thus, when pHzpc is greater than the pH of the solution (case of AC-BN), the adsorbent surface is positively charged to the point of electrostatically repulsing cationic GV [4]. Thus, when pHzpc is lower than the pH of the solution (case of AC-A), a strong GV attraction to the adsorbent surface is observed.

Through these results, it is observed that the electrostatic repulsions tend to mask or inhibit the textural properties of the adsorbents because AC-BN, which has a specific surface area and a total pore volume much greater than AC-A, has been less effective. in an alkaline medium. Thus, AC-A, despite its lesser textural properties, can be used to directly treat textile effluents which are generally basic [34].
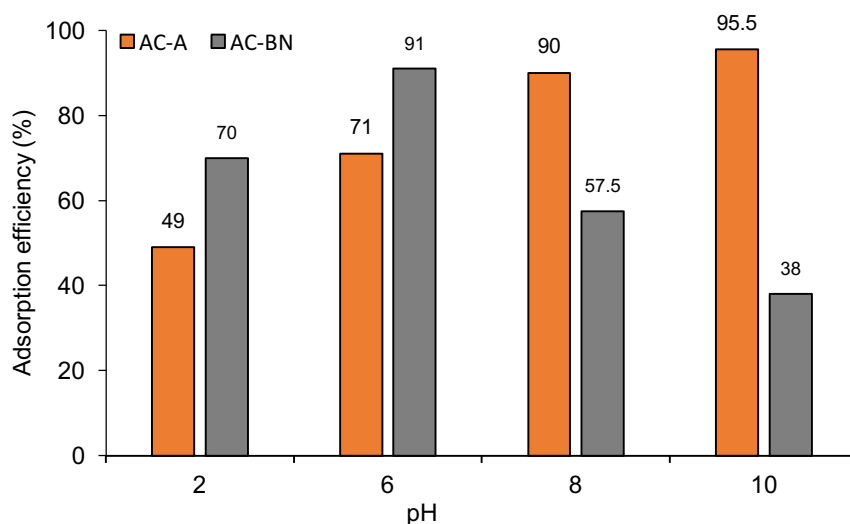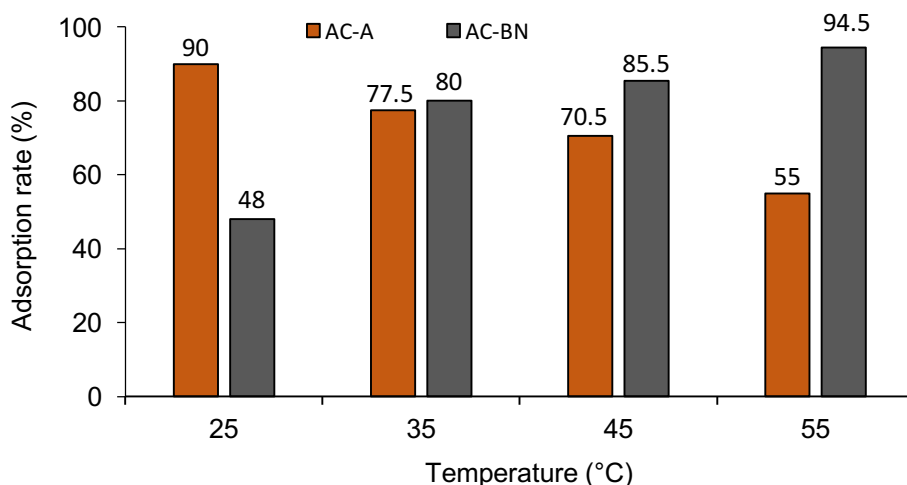

Figure 6. Effect of pH on the rate of GV reduction by AC-A and AC-BN (C_0 = 50 mg L^{-1}; V_0 = 100 mL; Time = 150 min; m_{AC} = 0.1 g and T = 25 °C)

3-4-3 Effect of Temperature

Figure 7 shows the effect of temperature on the Gentian Violet reduction rate by ACs. In fact, temperature is a very important parameter in the adsorption process to understand the exothermic or endothermic reactions between the adsorbent and the adsorbate. AC-A and AC-BN were used in GV solutions at temperatures ranging from 25 to 55 °C. The results of **Figure 7** show a crossed evolution because the GV removal rate decreases from 90 to 55% for the AC-A, whereas it increases from 48 to 94.5% concerning AC-BN. The decrease in adsorption capacity in addition to the increase in

temperature could be imputed to the weakening of the sorption forces between the active sites of the adsorbent and the ionic species of GV [35].

Figure 7. Effect of temperature on the rate of GV reduction by AC-A and AC-BN ($C_0 = 50$ mg L^{-1}; $V_0 = 100$ mL; Time = 150 min; $m_{AC} = 0.1$ g; pH = 7.2)

3-4-4 Effect of the mass of activated carbons

The adsorbent dose effect results (**Figure 8**) show that when the adsorbent dose increases, a remarkable adsorption of GV in solution follows. This removal increases from 60% to 94% (AC-A) and from 40% to 80% (AC-BN) for doses of 0.5 to 4 g L^{-1}. Indeed, increasing the adsorbent dose increases the number of active sites for further fixing the GV dye [36]. However, an excessive increase can inhibit the adsorption efficiency because adsorbent particles can coalesce, thereby preventing molecules from accessing porous sites [37]. This is the case with AC-BN where 2 g L^{-1} is the optimal dose because above this value, the reduction rate is stationary.
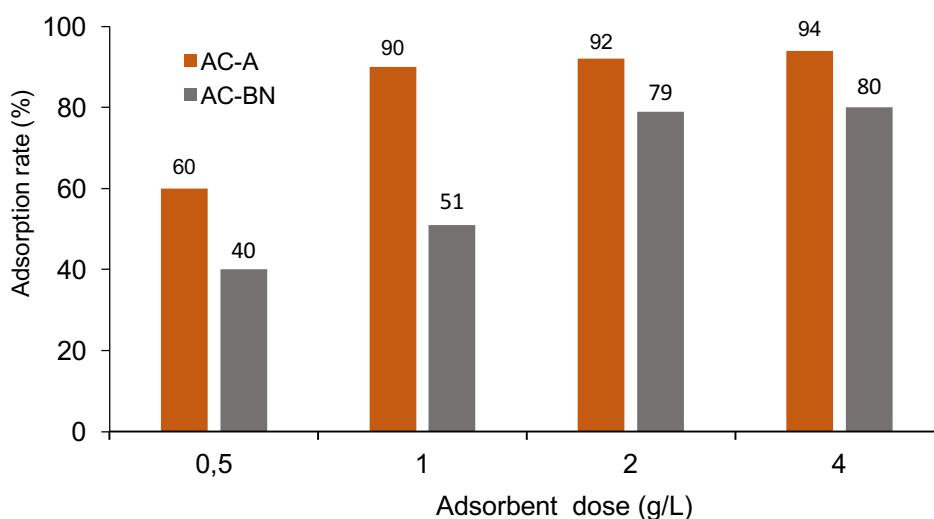
**Figure 8.** Effect of adsorbent dose on GV elimination (pH = 7.2; $C_0 = 50$ mg.L^{-1}; V = 100 mL; time = 150 min and T = 25 °C)

3-5 Adsorption mechanisms

3-5-1 Modelling of adsorption kinetics

The kinetics of GV adsorption by AC-A and AC-BN were modeled by using pseudo-first order and pseudo-second order non-linear regressions (**Figure 9**). The kinetic constants were obtained from

the slope and ordinate at the origin of the straight lines $\ln(q_e - q_t) = f(t)$ and $t/q_t = f(t)$. These non-linear models show that the experimental data are very close to those calculated by the pseudo-second order model and far apart from the pseudo-first order values. This is confirmed by the values of $q_{e,exp}$ and $q_{e,cal}$ according to the two models (**Table 2**). Furthermore, the coefficients of determination R^2 of the second-order model (0.993 and 0.999) are higher than those of the first order model (0.558 and 0.836) and tend towards unity. The values of χ^2 obtained (0.098 for AC-A and 0.051 for AC-BN) for the pseudo-second order model are all lower than those of χ^2 (572.075 for AC-A and 65.877 for AC-BN) of the pseudo-first order model. Therefore, pseudo-second order kinetics is the model that best describes the GV adsorption by each of the ACs. These different results suggest that the GV adsorption on AC-A and AC-BN is controlled by chemisorption [38]. Similar results were obtained when GV was removed by coal fly ash [39] and zeolite A [34].
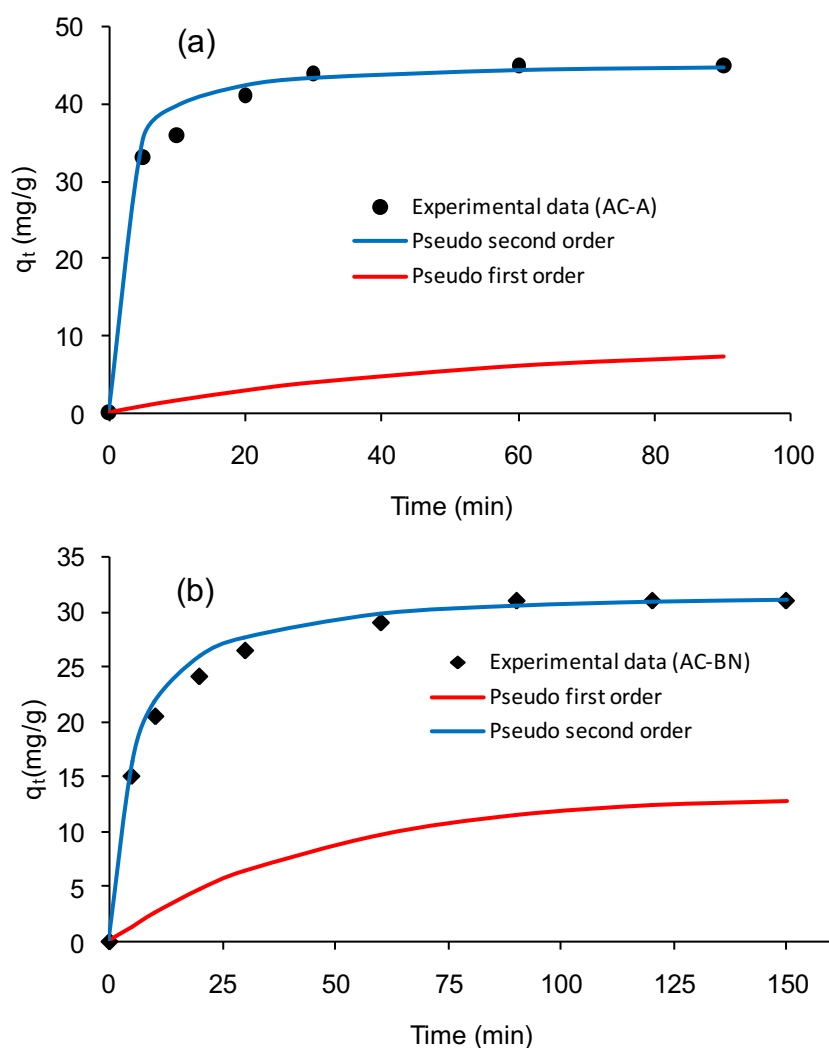

Figure 9. Kinetic models of GV adsorption by AC-A (a) and AC-BN (b) (C_0 = 50 mg L^{-1}; 0.1 g of AC; T = 25 °C; V = 100 mL; pH = 7.2)

Tableau 2. Parameters of the adsorption kinetics of GV on activated carbons

ACs	Pseudo first order					Pseudo second order			
	$q_{e,exp}$	k_1	$q_{e,cal}$	R^2	χ^2	k_2	$q_{e,cal}$	R^2	χ^2
	(mg g^{-1})	(min^{-1})	(mg g^{-1})			(g mg^{-1} min^{-1})	(mg g^{-1})		

AC-A	70	0.018	33.720	0.558	572.075	0.002	72.464	0.993 0.098
AC-BN	54	0.015	11.042	0.836	65.877	0.006	55.249	0.999 0.051

Intraparticle diffusion was studied to understand the kinetic mechanism of GV adsorption by the two activated carbons. Thus, the obtained curves (**Figure 10**) have two linearities that suggest the adsorption was carried out in two successive steps [40]. The first step (phase 1) corresponds to the gradual adsorption phase where intra-particulate diffusion is limiting. The second step (phase 2) corresponds to the absorption equilibrium for which the intra-particle diffusion is certainly slowed down because of the porous sites saturation and the molecular structure of GV. The fact that the fit line is not passing through the origin point implies that intra-particle diffusion is not the only mechanism that governs GV adsorption, but the adsorption rate is also influenced by diffusion outside of the particle [41]. Similar results were obtained by Laabd et al. [42] during the adsorption of benzene-1,2,4-tricarboxylic acid (trimellitic acid). The parameters of this intraparticle diffusion are recorded in **Table 3**.
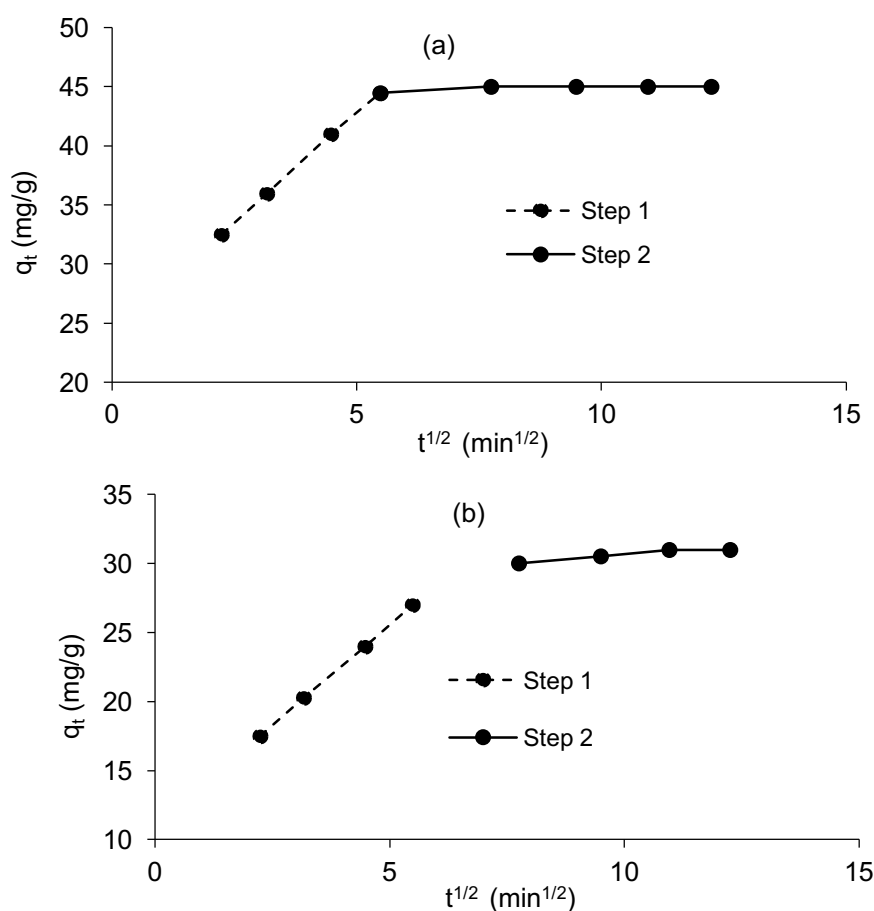
Figure 10. Kinetic intra-particle diffusion model of GV adsorption on AC-A (a) and AC-BN (b) ($C_0 = 50$ mg L^{-1}; time = 150 min; 1 g L^{-1} of AC and T = 25 °C)

Table 3. Gentian Violet intraparticle diffusion parameters on ACs

ACs	Phase 1			Phase 2		
	K_{id1}	C_1	R^2	K_{id2}	C_2	R^2
	(mg g^{-1} min$^{-1/2}$)	(mg g^{-1})		(mg g^{-1} min$^{-1/2}$)	(mg g^{-1})	

AC-A	3.718	24.236	**0.999**	0.037	44.534	**0.603**
AC-BN	1.120	17.482	**0.999**	0.037	23.534	**0.923**

These data confirm that step 1 is effectively progressive with rate constants (3.718 mg g^{-1} min$^{-1/2}$ for AC-A and 1.120 mg g^{-1} min$^{-1/2}$ for AC-BN) much higher than those of step 2 (0.037 mg g^{-1} min$^{-1/2}$ for AC-A and AC-BN).

3-5-3 Adsorption isotherms

The experimental data were fitted by using the nonlinear regressions of the Langmuir and Freundlich models (**Figure 11**). These adjustments were appreciated through the coefficients of determination (R^2). The inherent constants in these isotherms are reported in **Table 4**. According to these results, the values of R^2 of the Freundlich model are higher than those of Langmuir. In addition, the values of χ^2 of the Freundlich model are lower than those of Langmuir. This suggests that the GV elimination by these two activated carbons is perfectly described by Freundlich model. This adsorption is indeed favourable because Freundlich constant $1/n$ is between 0 and 1 [43]. Thus, this adsorption is characterized by a multilayer on the surface of each of the activated carbon.
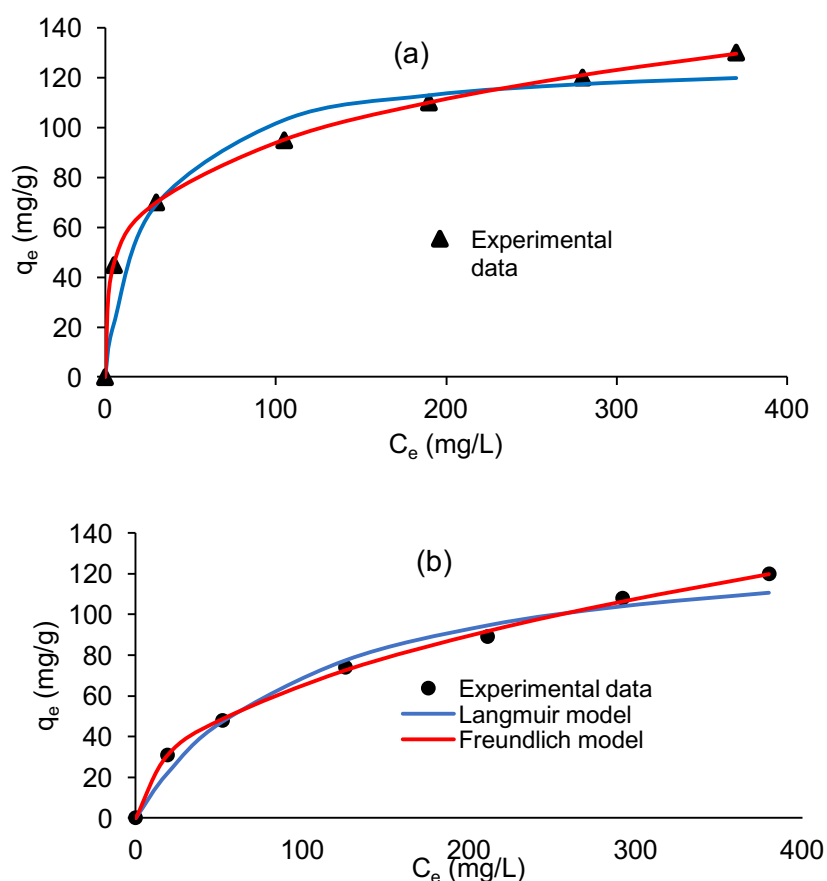

Figure 11. Nonlinear models of Langmuir and Freundlich isotherms for AC-A (a); AC-BN (b)

Table 4. Gentian Violet adsorption parameters by activated carbons (ACs) according to the linear Freundlich and Langmuir models

ACs	Freundlich model				Langmuir model			
	1/n	K_F (mg g^{-1}(L mg^{-1})$^{1/n}$)	R^2 (%)	χ^2	K_L (L mg^{-1})	q_m (mg g^{-1})	R^2 (%)	χ^2
AC-A	0.246	30.326	99.9	0.0095	0.039	128.04	98.0	29.410

| AC-BN | 0.453 | 8.113 | 99.8 | 0.145 | 0.0098 | 140.65 | 98.5 | 5.085 |

Values of the maximum adsorption capacities of GV (q_m) by AC-A and AC-BN are 128.04 mg g^{-1} and 140.65 mg g^{-1}, respectively. These values are higher than those obtained with ACs from coconut flowers (85.84 mg g^{-1}) [44], agricultural waste (92.59 mg g^{-1}) [45], FOR-140 (46.08 mg g^{-1}) [46], Zeolite A (10.67 mg g^{-1}) [34] and Bentonite (108.57 mg g^{-1}) [47] and show that ACs from mango shells are serious candidates for adsorption of this dye in industrial water.

3-6 Thermodynamic study of adsorption

The thermodynamic parameters (ΔH^0, ΔS^0 and ΔG^0) were obtained by plotting the linear regression of the graphical representation $\ln K_c$ as a function of $1/T$ (**Figure 12**). The different values are recorded in **Table 5**.
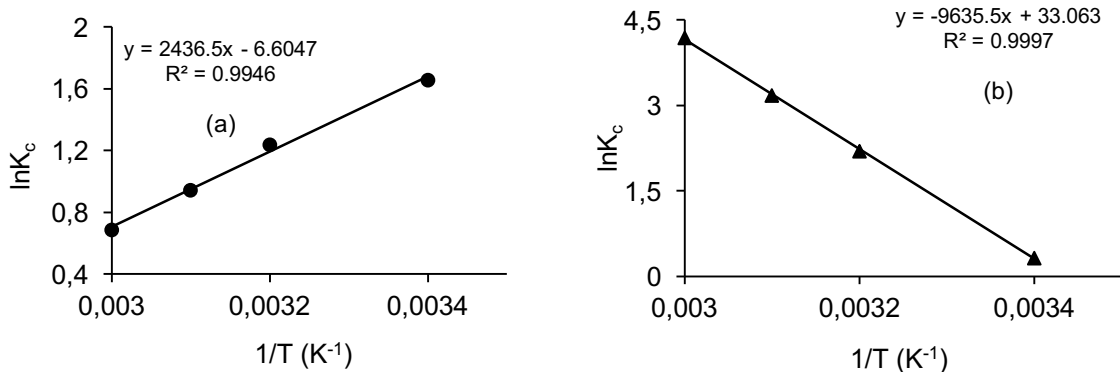
Figure 12. Thermodynamic absorption curves of GV on activated carbons: (a): AC-A, (b): AC-BN

Table 5. Thermodynamic parameters of Gentian Violet adsorption

ACs	Temperature (°C)	ΔG^0 (kJ mol^{-1})	ΔS^0 (kJ K^{-1} mol^{-1})	ΔH^0 (kJ mol^{-1})	R^2
AC-A	25	-4.108	-54.911	-20.257	0.995
	35	-3.167			
	45	-2.497			
	55	-1.870			
AC-BN	25	-0.800	274.886	80.110	0.999
	35	-5.626			
	45	-8.402			
	55	-11.411			

The results of **Table 5** show that ΔG^0 is negative at different temperatures for the two adsorbents (AC-A and AC-BN) and reflect the spontaneity of GV adsorption [48]. For AC-A, the values of ΔG^0 keep increasing with temperature, indicating that this adsorption is favourable at low temperature [48]. On the other hand, for the AC-BN adsorbent, the decrease in the values of ΔG^0 with the increase in temperature shows that the elimination of GV is favourable at high temperatures [49]. These results confirm those obtained in **Figure 7**. Furthermore, this GV adsorption process is exothermic for AC-A ($\Delta H^0 < 0$) and endothermic for AC-BN ($\Delta H^0 > 0$). The negative value of ΔS^0

indicates that the randomness at the solution/AC-A interface decreased during the adsorption process [50]. Thus, this disorder strongly increased at the solution/AC-BN interface (ΔS^0 positive).

Conclusion

Mango shells activated with phosphoric acid or sodium hydroxide afforded two activated carbons with different textural and morphological properties. These two activated carbons developed more mesopores, with specific surfaces of 270 $m^2 g^{-1}$ for AC-A and 421 $m^2 g^{-1}$ for AC-BN. Functional groups and pHzpc strongly influenced Gentian Violet adsorption on the surface of the activated carbons. For these two activated carbons, Gentian Violet adsorption was perfectly described by Freundlich model and pseudo-second order kinetics. The spontaneity of the Gentian Violet adsorption was revealed by the negative values of ΔG^0 with endothermic and exothermic effects for AC-BN and AC-A, respectively. Finally, these two adsorbents may be used for the depollution of textile wastewater generally loaded with dyes.

References

[1] B.G.H. Briton, B.K. Yao, Y. Richardson, L. Duclaux, L. Reinert, Y. Soneda, Optimization by Using Response Surface Methodology of the Preparation from Plantain Spike of a Micro-/Mesoporous Activated Carbon Designed for Removal of Dyes in Aqueous Solution, *Arabian Journal for Science and Engineering* 45(9) (2020) 7231-7245. doi:10.1007/s13369-020-04390-0

[2] A. Oussalah, A. Boukerroui, A. Aichour, B. Djellouli, Cationic and anionic dyes removal by low-cost hybrid alginate/natural bentonite composite beads: Adsorption and reusability studies, *Int J Biol Macromol.* 124 (2019) 854–862. doi:10.1016/j.ijbiomac.2018.11.197

[3] R. Croce, F. Cinà, A. Lombardo, G. Crispeyn, C.I. Cappelli, M. Vian, S. Maiorana, E. Benfenati, D. Baderna, Aquatic toxicity of several textile dye formulations: Acute and chronic assays with Daphnia magna and Raphidocelis subcapitata, *Ecotoxicol Environ Saf.* 144 (2017) 79–87. doi:10.1016/j.ecoenv.2017.05.046

[4] K. Nadeem, G.T. Guyer, B. Keskinler, N. Dizge, Investigation of segregated wastewater streams reusability with membrane process for textile industry, *Journal of Cleaner Production* 228 (2019) 1437–1445. https://doi.org/10.1016/j.jclepro.2019.04.205

[5] H. Fan, Y. Ma, J. Wan, Y. Wang, Removal of gentian violet and rhodamine B using banyan aerial roots after modification and mechanism studies of differential adsorption behaviors, *Environ Sci Pollut Res Int.* 27 (2020) 9152–9166. doi:10.1007/s11356-019-07024-7

[6] S. Shoukat, H.N. Bhatti, M. Iqbal, S. Noreen, Mango stone biocomposite preparation and application for crystal violet adsorption: A mechanistic study, *Microporous and Mesoporous Materials* 239(C) (2017) 180–189. doi:10.1016/j.micromeso.2016.10.004

[7] S.P. Ghuge, A.K. Saroha, Catalytic ozonation of dye industry effluent using mesoporous bimetallic Ru-Cu/SBA-15 catalyst, *Process Safety and Environmental Protection* 118 (2018) 125–132. https://doi.org/10.1016/j.psep.2018.06.033

[8] J. Ano, A.S. Assémian, Y.A. Yobouet, K. Adouby, P. Drogui, Electrochemical removal of phosphate from synthetic effluent: A comparative study between iron and aluminum by using experimental design methodology, *Process Safety and Environmental Protection* 129 (2019) 184–195. https://doi.org/10.1016/j.psep.2019.07.003

[9] S. Wong, H.H. Tumari, N. Ngadi, N.B. Mohamed, O. Hassan, R. Mat, N.A.S. Amin, Adsorption of anionic dyes on spent tea leaves modified with polyethyleneimine (PEI-STL), *Journal of Cleaner Production* 206 (2019) 394–406. https://doi.org/10.1016/j.jclepro.2018.09.201

[10] V. da Silva Lacerda, J.B. López-Sotelo, A. Correa-Guimarães, S. Hernández-Navarro, M. Sánchez-Báscones, L.M. Navas-Gracia, P. Martín-Ramos, J. Martín-Gila, Rhodamine B removal with activated carbons obtained from lignocellulosic waste, *Journal of Environmental Management* 155 (2015) 67–76. https://doi.org/10.1016/j.jenvman.2015.03.007

[11] J. Lin, R. Choowang, G. Zhao, Fabrication and characterization of activated carbon fibers from oil palm trunk, *Polymers* 12(12) (2020) 2775. https://doi.org/10.3390/polym12122775

[12] Q. Liang, Y. Liu, M. Chen, L. Ma, B. Yang, L. Li, Q. Liu, Optimized preparation of activated carbon from coconut shell and municipal sludge, *Materials Chemistry and Physics* 241 (2020) 122327. https://doi.org/10.1016/j.matchemphys.2019.122327

[13] S. Wang, H. Nam, H. Nam, Preparation of activated carbon from peanut shell with KOH activation and its application for H2S adsorption in confined space, *Journal of Environmental Chemical Engineering* 8(2) (2020) 103683. doi:10.1016/j.jece.2020.103683

[14] S. Benhabiles, K. Rida, Production of efficient activated carbon from sawdust for the removal of dyes in single and binary systems–a full factorial design, *Particulate Science and Technology* 39(2) (2021) 237–251. https://doi.org/10.1080/02726351.2019.1711475

[15] R. Sahmarani, S. Net, C. Chbib, M. Baroudi, B. Ouddane, Elimination of organochlorine pesticides from water by a new activated carbon prepared from Phoenix dactylifera date stones, *Environ Sci Pollut Res Int* 28(8) (2021) 10140–10154. doi:10.1007/s11356-020-11445-0

[16] T. Abdoulaye, S. Souleymane, K.M. Liliane, T.C. Drissa, Z.A. Fabrice, S.Y. Réné, Morphological and Physicochemical Parameters of Three Mango (Mangifera Indica L) Varieties Exported In North of Ivory Coast, *EAS J Nutr Food Sci.* 2(5) (2020) 298–303. doi:10.36349/easjnfs.2020.v02i05.008

[17] O.O. Awolu, B. Manohar, Quantitative and qualitative characterization of mango kernel seed oil extracted using supercritical CO_2 and solvent extraction techniques, *Heliyon* 5 (2019) e03068. https://doi.org/10.1016/j.heliyon.2019.e03068

[18] A.B.B. Kassi, Y. Soro, E.N. Koffi and S. Sorho, Physicochemical study of kernel oils from ten varieties of Mangifera indica (Anacardiaceae) cultivated in Cote d'Ivoire, *African Journal of Food Science* 13(7) (2019) 135-142. DOI:10.5897/AJFS2019.1827

[19] A.B.B. Kassi, Y. Soro, B. Fante, K.J. Golly, S. Sorho, A.S. Toure and J-M. Coustard, Isolation and identification of bioactive compounds from kernel seed cake of the mango (*Mangifera indica* Lam), *Int. J. Biol. Chem. Sci.* 8(4) (2014) 1885-1895.

[20] T. Abdoulaye, Z.A. Fabrice, T. Naka, S. Fatou, S.Y. Réné, C. Adama, Physicochemical and nutritive properties of by-products flours from cashew (*Anacardium occidentale*) and mango (*Mangifera indica*) for ruminants feeding in Poro region (Northern Côte d' Ivoire), *EAS Journal of Nutrition and Food Sciences* 2(2) (2020) 44–48. doi:10.36349/easjnfs.2020.v02i02.003

[21] R.C. de Andrade, R.S.G. Menezes, R.A. Fiuza-Jr, H.M.C. Andrade, Activated carbon microspheres derived from hydrothermally treated mango seed shells for acetone vapor removal, *Carbon Letters* 31(4) (2020) 1-15. https://doi.org/10.1007/s42823-020-00184-4

[22] I.O. Okeowo, E.O. Balogun, A.J. Ademola, A.O. Alade, T.J. Afolabi, E.O. Dada, A.G. Farombi, Adsorption of Phenol from Wastewater Using Microwave-Assisted Ag–Au Nanoparticle-Modified Mango Seed Shell-Activated Carbon, *International Journal of Environmental Research* 14 (2020) 215–233. doi:10.1007/s41742-020-00244-7

[23] A.A. Olu, D.E. Olujimi, O.O. Abel, O.I. Olanrewaju, A.A. Olanrewaju, A.T. Jolade, Adsorption of Methylene Blue from Aqueous Solution using Microwave-Assisted $BaCl_2$ Modified Activated Carbon Produced from Mango Seed Shell, *LAUTECH Journal of Civil and Environmental Studies* 3(1) (2019) 72-82. DOI: 10.36108/laujoces/9102/20(0270)

[24] B.A. Olufemi, F. Otolorin, Comparative adsorption of crude oil using mango (Mangnifera indica) shell and mango shell activated carbon, *Environ Eng Res.* 22(4) (2017) 384–392. DOI: https://doi.org/10.4491/eer.2017.011

[25] A. Zubrik, M. Matik, S. Hredzák, M. Lovás, Z. Danková, M. Kováčová, J. Briančin, Preparation of chemically activated carbon from waste biomass by single-stage and two-stage pyrolysis, *Journal of Cleaner Production* 143(C) (2017) 643–653. doi:10.1016/j.jclepro.2016.12.061

[26] Y. Kan, Q. Yue, D. Li, Y. Wu, B. Gao, Preparation and characterization of activated carbons from waste tea by H_3PO_4 activation in different atmospheres for oxytetracycline removal, *Journal of the Taiwan Institute of Chemical Engineers* 71 (2017) 494–500. https://doi.org/10.1016/j.jtice.2016.12.012

[27] H. Padhiyar, A. Thanki, N.K. Singh, S. Pandey, M. Yadav, T.C. Yadav, Parametric and kinetic investigations on segregated and mixed textile effluent streams using Moringa oleifera seed powders of different sizes, *Journal of Water Process Engineering* 34 (2020) 101159. https://doi.org/10.1016/j.jwpe.2020.101159

[28] N. Ayawei, A.N. Ebelegi, D. Wankasi, Modelling and Interpretation of Adsorption Isotherms, *Journal of Chemistry* 2017 (2017) 1-11. https://doi.org/10.1155/2017/3039817

[29] C. Yang, L. Guan, J. Wang, X. Yang, M. Lin, G. You, S. Tan, X. Yu, M. Ge, Enhanced fluoride removal behaviour and mechanism by dicalcium phosphate from aqueous solution, *Environmental Technology (United Kingdom)* 40(28) (2019) 3668–3677. https://doi.org/10.1080/09593330.2018.1484523

[30] A.K. Shakya, R. Bhande, P.K. Ghosh, A practical approach on reuse of drinking water treatment plant residuals for fluoride removal, *Environmental Technology (United Kingdom)* 41(22) 2020 2907-2919. https://doi.org/10.1080/09593330.2019.1588383

[31] X. Borgohain, A. Boruah, G.K. Sarma, M.H. Rashid, Rapid and extremely high adsorption performance of porous MgO nanostructures for fluoride removal from water, *Journal of Molecular Liquids* 305 (2020) 112799. https://doi.org/10.1016/j.molliq.2020.112799

[32] J. Wagn, G.-Y. Hou, L.-K. Wu, H.-Z. Cao, G.-Q. Zheng, Y.-P. Tang, A novel adsorbent of three-dimensional ordered macro/mesoporous carbon for removal of malachite green dye, *Journal of Central South University* 27 (2020) 388–402. doi.org/10.1007/s11771-020-4304-3

[33] K.A.G. Gusmão, L.V.A. Gurgel, T.M.S. Melo, L.F. Gil, Application of succinylated sugarcane bagasse as adsorbent to remove methylene blue and gentian violet from aqueous solutions - Kinetic and equilibrium studies, *Dyes and Pigments.* 92 (2012) 967–974. https://doi.org/10.1016/j.dyepig.2011.09.005

[34] Jumaeri, E. Kusumastuti, S.J. Santosa, Sutarno, Adsorption of Crystal Violet Dye Using Zeolite A Adsorption of Crystal Violet Dye Using Zeolite A Synthesized From Coal Fly Ash, *Mater. Sci. Eng.* 172 (2017) 1-8. doi:10.1088/1757-899X/172/1/012028

[35] A.E. Ofomaja, Y.-S. Ho, Equilibrium sorption of anionic dye from aqueous solution by palm kernel fibre as sorbent, *Dyes and Pigments* 74(1) (2007) 60–66. doi:10.1016/j.dyepig.2006.01.014

[36] V. V. Gedam, P. Raut, A. Chahande, P. Pathak, Kinetic, thermodynamics and equilibrium studies on the removal of Congo red dye using activated teak leaf powder, *Applied Water Science* 9 (2019) 55. https://doi.org/10.1007/s13201-019-0933-9

[37] C.A. Igwegbe, A.E. Al-Rawajfeh, H.I. Al-Itawi, S. Sharadqah, S. Al-Qazaqi, E.A. Hashish, M. Al-Qatatsheh, M. Sillanpaa, Utilization of calcined gypsum in water and wastewater treatment: Removal of phenol, *J. Ecol. Eng.* 20 (2019) 1–10. DOI: doi.org/10.12911/22998993/108694

[38] N.M. Mahmoodi, O. Masrouri, Cationic Dye Removal Ability from Multicomponent System by Magnetic Carbon Nanotubes, *J. Solution Chem.* 44 (2015) 1568 doi:10.1007/s10953-015-0366-5

[39] T.C.R. Bertolini, J.C. Izidoro, C.P. Magdalena, D.A. Fungaro, Adsorption of Crystal Violet Dye from Aqueous Solution onto Zeolites from Coal Fly and Bottom Ashes, *Orbital: Electron. J. Chem.* 5(3) (2013) 179–191. doi:10.17807/orbital.v5i3.488

[40] E. Lorenc-Grabowska, G. Gryglewicz, Adsorption of lignite-derived humic acids on coal-based mesoporous activated carbons, *J Colloid Interface Sci.* 284(2) (2005) 416–423. doi:10.1016/j.jcis.2004.10.031

[41] Q. Chang, Colloid and Interface Chemistry of Water Quality Control, 1st Edition, Academic Press, Hardcover ISBN: 9780128093153, eBook ISBN: 9780128093191 (2016) doi: 10.1016/B978-0-12-809315-3/00010-4

[42] M. Laabd, H. Chafai, A. Essekri, M. Elamine, S.A. Al-Muhtaseb, R. Lakhmiri, A. Albourine, Single and multi-component adsorption of aromatic acids using an eco-friendly polyaniline-based biocomposite, *Sustainable Materials and Technologies* 12(C) (2017) 35–43. doi:10.1016/j.susmat.2017.04.004

[43] M.A. Sabrina, Utilisation des déchets agro-industriels pour l'élimination du chrome hexavalent en solution aqueuse: Thèse de Doctorat en Chimie, Université Mouloud Mammeri de Tizi-Ouzou, République algérienne démocratique et populaire (2018) 179 P.

[44] S. Senthilkumaar, P. Kalaamani, C. V. Subburaam, Liquid phase adsorption of Crystal violet onto activated carbons derived from male flowers of coconut tree, *J Hazard Mater.* 136(3) (2006) 800–808. doi:10.1016/j.jhazmat.2006.01.045

[45] B.H. Hameed, Equilibrium and kinetic studies of methyl violet sorption by agricultural waste, *J Hazard Mater.* 154(1-3) (2008) 204–212. doi:10.1016/j.jhazmat.2007.10.010

[46] W. Fortas, A. Djelad, M.A. Hasnaoui, M. Sassi, A. Bengueddach, Adsorption of gentian violet dyes in aqueous solution on microporous AlPOs molecular sieves synthesized by ionothermal method, *Mater. Res. Express.* 5(2) (2018) 025018. http://dx.doi.org/10.1088/2053-1591/aaaac2

[47] K. Bellir, I. Sadok Bouziane, Z. Boutamine, M. Bencheikh Lehocine, A.H. Meniai, Sorption Study of a Basic dye "Gentian Violet" from Aqueous Solutions Using Activated Bentonite, *Energy Procedia* 18 (2012) 924–933. https://doi.org/10.1016/j.egypro.2012.05.107

[48] S. Mondal, K. Sinha, K. Aikat, G. Halder, Adsorption thermodynamics and kinetics of ranitidine hydrochloride onto superheated steam activated carbon derived from mung bean husk, *Journal of Environmental Chemical Engineering* 3(1) (2015) 187–195. doi.org/10.1016/j.jece.2014.11.021

[49] M.P. Tavlieva, S.D. Genieva, V.G. Georgieva, L.T. Vlaev, Kinetic study of brilliant green adsorption from aqueous solution onto white rice husk ash, *Journal of Colloid and Interface Science* 409 (2013) 112–122. https://doi.org/10.1016/j.jcis.2013.07.052

[50] Y. Li, Q. Du, T. Liu, X. Peng, J. Wang, J. Sun, Y. Wang, S. Wu, Z. Wang, Y. Xia, L. Xia, Comparative study of methylene blue dye adsorption onto activated carbon, graphene oxide, and carbon nanotubes, *Chemical Engineering Research and Design* 91(2) (2013) 361–368. https://doi.org/10.1016/j.cherd.2012.07.007

(2021) ; http://www.jmaterenvironsci.com